Organic Complementary Inverters Based on Vertical-Channel Dual-Base Thin-Film Transistors with Time Constants < 10ns

Zhongbin Wu (zhongbinwu@outlook.com)
Technische Universität Dresden https://orcid.org/0000-0002-8425-5013
Erjuan Guo
TU Dresden
Shen Xing
TU Dresden
Felix Dollinger
Technische Universität Dresden https://orcid.org/0000-0003-4904-0276
René Hübner
Helmholtz-Zentrum Dresden-Rossendorf (HZDR)
Shu-Jen Wang
TU Dresden
Karl Leo (karl.leo@tu-dresden.de)
TU Dresden
Hans Kleemann
TU Dresden

Article

Keywords: vertical transistors, OTFTs, OPBTs, dual-gate/base, complementary inverters

Posted Date: September 17th, 2020

DOI: https://doi.org/10.21203/rs.3.rs-74486/v1

Version of Record: A version of this preprint was published at Nature Electronics on July 15th, 2021. See the published version at https://doi.org/10.1038/s41928-021-00613-w.

Abstract

Lateral-channel dual-gate organic thin-film transistors (OTFTs) are utilized in organic pseudo-CMOS inverters to realize switching voltage control. However, the relatively long channel length will slow the inverter operation. Vertical-channel dual-gate OTFTs are an attractive alternative due to the short channel length. In this work, controllable and reliable complementary inverters are presented using vertical n-channel organic permeable dual-base transistors (OPDBTs) and vertical p-channel organic permeable base transistors (OPBTs). With operating voltages < 2.0 V, the threshold voltages of the n-type OPDBTs are changed across a wide range from 0.12 to 0.82 V by varying the voltage of the additional base. The fabricated tunable organic complementary inverter features switching voltage shift and gain enhancement. In addition, the inverters show very small switching time constants (< 10 ns) at 10 MHz. Our work represents a significant step towards the application of vertical dual-gate/base transistors in power-efficient organic complementary inverters, offering the capability to easily tune the switching voltage of organic complementary inverters. This facilitates the development of high-performance and complex organic digital integrated circuits.

Introduction

Organic thin-film transistors (OTFTs) have attracted considerable attention for realizing numerous applications in large-area electronics, such as electronic-paper displays, microprocessors, radio-frequency identification circuits, flexible sensors, and electronic skins[1–5]. An essential electronic build blocking for practically any kind of digital circuitry are logic gates and in particular inverters circuits. Ideally, they are characterized by a low driving voltage, low static and dynamic power uptake, high gain, and fast response time in order to enable complex and power-efficient devices. In general, low driving voltage of OTFTs may be achieved using high capacitance dielectric layers and reducing the density of the sub-gap density-of-states in the channel. However, a low static and dynamic power uptake, high signal integrity, and high gain of an organic semiconductor based inverter is a far more difficult target to reach. The best strategy to achieve the above-described goals is to use a complementary circuit technology composed of p-type and n-type transistors. Compared to unipolar inverters where a power is constantly dissipated through the load resistance, complementary circuits offer a significantly reduced static and dynamic power uptake because one transistor operates in its off-state. However, in order to obtain complementary inverters with a high gain, large noise margin and good signal integrity, it is essential to have balanced charge carrier transport in the n-type and p-type transistors. In this regard, the threshold voltage (V_{TH}) is of particular importance because it determines the trip point of the inverter, which is the input bias at which the gate inverts the output signal. For standard silicon complementary metal-oxide-semiconductor transistors (CMOS), the threshold voltage at the onset of inversion can be accurately set by the amount of doping applied by ion implantation[6].

Although channel doping has been successfully demonstrated in organic transistors[7–9], it may not be the best strategy for threshold voltage tuning in OTFTs due to deterioration of charge carrier mobility,

reduction of on/off-ratio, or insufficient controllability. An alternative method for threshold voltage tuning is the use of dual-gate transistors. In this case, a second gate electrode is used to precisely set the threshold voltage. The practical implantation of dual-gate transistors and control of V_{TH} of OTFTs have been reported by several groups. In 2005, the organic dual-gate TFTs based on pentacene were reported by Cui and Liang[10]. During the same year, Iba et al.[11], Gelinck et al.[12], Chua et al.[13], and Morana et al.[14] published improved dual-gate transistors. Since then, numerous papers on organic dual-gate TFTs appeared in literature. In addition, the change of V_{TH} of an OTFT with a dual-gate is precisely elucidated by an analysis of the electrostatic potential[14]. Morana et al. showed that the input-output characteristics of the inverter change upon applying a bias to the top gate of the driver. A dual-gate inverter with back-gates on both the load and driver transistor was reported by Spijkman et al. in 2008[15]. A comprehensive study of the use of dual-gate transistors to control the threshold voltage of the load transistor and drive transistor of inverters and digital circuits was performed by Myny et al. in 2011[16]. Furthermore, dual-gate TFTs are integrated in complementary technologies to increase the noise margin which consequently can lower the operation voltage of the complementary inverters.

All the inverters discussed above are based on lateral-channel dual-gate OTFTs. However, due to the micrometer-long channel length, the limits of the contact resistance, and the large capacitance in the lateral-channel dual-gate devices, it is a substantial challenge to further increase the operation frequency without employing costly high-resolution patterning techniques[17,18]. Vertical organic transistor architecture though, offers sub-micrometer channel devices enabling low-voltage and high-transconductance operation[19]. In particular, the performance and stability of vertical organic transistors has been improved significantly in recent years due to advancements in device manufacturing as well as improvements of the layer structure[20–28]. One vertical organic transistor structure that stands out of all proposed approaches is the organic permeable base transistor (OPBT) which is the organic transistor with the highest transition frequency reported[29]. Furthermore, OPBTs show excellent stability comparable to the best lateral OTFTs[30]. However, complementary inverter circuits based on vertical organic transistors have not been reported so far which is mainly caused by the lack of proper p- or n-type transistors. Thus, so far vertical organic transistors have never proven their advantages in terms of high-frequency operation in functional circuits.

In this study, we report, for the first time, the fabrication and measurements of organic complementary inverters with vertical-channel dual-gate TFTs. We demonstrate a complementary inverter using n-type organic permeable dual-base transistors (OPDBTs) and p-type OPBTs. The threshold voltage of n-type OPDBTs can be adjusted by applying a bias on the second base. Finally, the proposed complementary inverters show reliable output curves and switching voltage tunability by independently adjusting the applied base bias of the n-type OPDBTs. In addition, the organic inverters can maintain the switching states above 10 MHz with time constants for the fall and rise time of less than 10 ns. With these performance measures, the complementary inverters proposed in this work set a new record for the switching rate of low-voltage organic logic circuits. Moreover, this work proves that the vertical organic transistor concept is a suitable strategy to further improve the performance of organic electronic circuits.

Results

Transistor design. Figure 1 shows a schematic illustration of the organic complementary inverter consisting of an n-type OPDBT and a p-type OPBT. OPBTs resemble a triode-like structure and hence instead of the gate, the control electrode is named as the base. In an OPDBT or an OPBT, organic semiconductor layers are embedded between the collector electrode (C), emitter electrode (E), and base electrode (B). Typically, the layer thicknesses of the collector and emitter are 100 nm aluminum (Al), with an additional layer of 20 nm chromium (Cr) for n-type OPDBTs, or 20 nm gold (Au) for p-type OPBTs. As organic semiconductor materials, C_{60} and pentacene are used for the n-type OPDBT and the p-type OPBT, respectively. A 20-nm-thick layer of C_{60} doped with the strong electron donor $W_2(hpp)_4$ (n-C_{60}, dopant concentration of 1.0 wt.%) inserted underneath the emitter is used to reduce the contact resistance and enable the Ohmic-like injection of electrons from the metal electrode in n-type OPDBTs.[31] A 50-nm-thick layer of pentacene doped with the p-dopant F6TCNNQ is also used to reduce the contact resistance between the metal and organic semiconductors, and thus to enhance the injection of holes from the emitter of p-type OPBTs.[31] The base electrode in an OPBT consists of a 15-nm-thick aluminum film which, due to intentional oxidation, is covered with a native 2–3 nm thin Al_2O_3 layer.[20] Furthermore, due to the mechanical strain during the oxidation process, nanometer-size pinholes open up in the base and enable charge carrier transport from the emitter to the collector. Details on the device fabrication are given in the Experimental Section. The properties of the base layer are investigated by transmission electron microscopy (TEM) and the detailed explanation can be found in Supplementary Fig. S1.

In an OPBT, charge carriers are injected from the emitter electrode into the organic semiconductor material by applying an emitter-collector voltage. When a positive base bias (negative bias for p-type OPBTs) is applied, the OPBT is turned on, and the charge carriers from the emitter are accumulated at the Al_2O_3 of the base. Once accumulated, electrons (or holes) will laterally diffuse to the pinholes in the base, and then be pulled from the pinholes to the collector. If the base-emitter voltage is not applied, electrons (or holes) cannot pass through the base and therefore cannot reach the collector. Consequently, the OPBT is in its off-state. In an OPDBT, the second base will also control the transport of charge carriers. Charge carriers can go through the pinholes in both base electrodes and reach the collector only when the potential of base1 is non-zero and the potential of base2 is larger than that of base1[32].

Electrical characterization of n- and p-type transistors. All electrical measurements of the transistors are carried out in ambient air with encapsulation at room temperature. Figures 2a and b show the electrical characteristics of an n-type OPDBT. The transfer curves are measured as a function of base2-emitter voltage (V_{B2}) at different base1-emitter voltages (V_{B1}) of 0, 0.5, 1.0, 1.5 and 2.0 V, respectively. The corresponding performance parameters of the transfer curves, e.g., transmission values ($I_C/(I_C+I_B)$), on-currents, on/off ratios, threshold voltages (V_{TH}), subthreshold swing (SS), and current gain ($\beta = I_C/I_B$) are extracted and summarized in the Supplementary Table S1. When V_{B1} = 0 V, the OPDBT stays in its off-state. As V_{B1} increases from 0 to 0.5 V, it can be turned on. The on-current increases from 0.96 to 4.06 mA as V_{B1} increases from 0.5 to 2.0 V. Furthermore, a transmission value of 99.999%, an on/off ratio of 4.7 ×

10^4, a subthreshold swing of 123 mV dec^{-1}, and a current gain of 2×10^7 are achieved when V_{B1} reaches 2.0 V. Importantly, the threshold voltages of the OPDBT shift from 0.12 to 0.82 V when V_{B1} increases from 0.5 to 2.0 V (see Supplementary Fig. S2)[30]. Thus, by changing the applied base1 voltages, the threshold voltage of the OPDBTs can be set at a desired value. Figure 2b shows the output characteristics of the n-type OPDBTs. A small undesirable nonlinearity of the collector current at small collector-emitter voltages can be observed, which is caused by the space-charge-limited current in the organic semiconductor layer[33]. Overall, the performance of OPDBTs is comparable to single-base devices showing a transition frequency of 40 MHz[29]. The larger overall layer thickness for dual-base devices though caused the current to be slightly lower. The electrical characteristics of a p-type OPBT are shown in Figs. 2c, d, and the corresponding performance parameters are summarized in Supplementary Table S2. An on-current of 5.28 mA, a transmission value of 99.87%, an on/off ratio of 5×10^3, a subthreshold swing of 258 mV dec^{-1}, and a current gain of 9×10^3 are achieved as shown in Fig. 2c. The output characteristics of p-type OPBTs are measured and presented in Fig. 2d. According to the output curves in the linear region, the semiconductor/electrode contact is Ohmic rather than Schottky-like. I_C shows good saturation in the output curves. Overall, the performance of the n- and p-type transistors is quite nicely balanced.

Application in complementary inverters. Using an n-type OPDBT and a p-type OPBT, we realize an organic complementary inverter. The complementary inverter circuit is assembled as shown in Fig. 1 and Fig. 3a. The p-type OPBT is connected through its emitter electrode to the positive supply voltage (V_{CC}) and by the collector electrode to the output terminal. The n-type OPDBT is also connected by the collector electrode to the output terminal and by the emitter to the ground. The base2 electrode of the n-type OPDBT is connected to the base electrode of the p-type OPBT and the input signal. The static voltage transfer curves of the inverter for different supply voltages at constant control voltage ($V_{Control}$) of 2.0 V are presented in Figs. 3b and c. With different supply voltages, remarkable inverter characteristics and excellent gains of 16.4–28 are achieved, which is comparable to the organic inverters with lateral-channel transistors[34–36]. The tripping point of the inverter is not at its ideal position $V_{CC}/2$ due to the difference in the threshold voltage of the n- and p-type transistor. However, as we will show later, this effect can be reduced using the function of the OPDBT.

In addition, the dynamic response characteristics of the present inverter are evaluated by applying a square-wave input signal with an amplitude (V_{IN}) of 2.0 V (adjusting the supply and control voltage so that $V_{CC} = V_{Control}$ = 2.0 V), and frequencies (f) of 1 and 10 MHz, respectively. The results are shown in Figs. 3d and e, where the black and red curves indicate the input voltage V_{IN} and output voltage V_{OUT}, respectively. The output voltage exhibits an inverter response to the input voltage with a transient behavior just after the changes in V_{IN}. The high output almost reaches 2.0 V (V_{CC}), and the low output closely reaches 0 V at a frequency of 1 MHz as well. With the increase of the frequency to 10 MHz, the output voltage slightly drops, but it is also close to 2.0 V, and the state of the inverter can still be maintained. The rise (τ_{rise}) and fall (τ_{fall}) time constants of the switching events at different supply voltages are plotted in Fig. 3 f. τ_{rise} and τ_{fall} are defined as a time from 10 to 90% of the change between

the two steady-state values (see Supplementary Fig. S3). The smallest time constants of 5 ns and 6 ns are observed at a supply voltage of 4.0 V. To date, organic unipolar inverters reported by Borchert et al. show the smallest time constants of 19 ns and 56 ns, which are achieved at a frequency of 2 MHz and a supply voltage of 2.5 V[37]. However, the gain of these inverter structures is smaller than 10. Therefore, complementary inverters based on OPBTs allow the dynamic performance of the organic inverters to reach a higher frequency, and respond a smaller time constants, and operate with a higher gain.

Finally, the effect of the additional base electrode in an OPDBT on the transfer characteristics of the complementary inverter is investigated (see Fig. 4). A supply voltage of 3.5 V is applied and $V_{Control}$ is ranged from 0.5 to 2.0 V. As can be seen, varying $V_{Control}$ from 0.5 to 2.0 V causes the threshold voltages of the n-type OPDBTs and hence the switching voltage of the inverter to shift systematically toward more positive voltages. In this way, dual-base transistors enable a wide-range of switching voltage controllability of a complementary inverter over 0.8 V at an input voltage < 2.0 V in a deterministic manner. The highest gain of 28.2 is achieved when $V_{Control}$ = 0.5 V, which can be attributed to the highest threshold swing value of 113 mV dec^{-1}. Hence, a switching voltage tunable inverter circuit is realized by using a V_{TH} tunable n-type OPDBT and a p-type OPBT.

Conclusions

In summary, this work constitutes the first application of vertical dual-base transistors to form low-voltage organic complementary inverters. The threshold voltage control of an n-type OPDBT is shown, and this technique is applied to tune the switching voltage of organic complementary inverters. Furthermore, dual-base transistors enable a wide-range of switching voltage controllability of a complementary inverter of over 0.8 V at an input voltage < 2.0 V. Remarkably, the complementary inverters can maintain the switching states and operate with small time constants of < 10 ns at 10 MHz, showing great promises for complex electronic circuits.

Methods

Device fabrication. Both the n-type organic permeable dual-base transistors (OPDBTs) and p-type single-base OPBTs presented are fabricated in a single chamber UHV-tool. The glass substrate is previously cleaned with N-Methylpyrrolidone, deionized water, ethanol, and ultraviolet ozone cleaning system. By using thermal vapor deposition under ultrahigh-vacuum conditions, the layer stack (see Fig. 1) is realized by subsequent deposition of thin films through a set of shadow masks. The deposition system includes a wedge for realizing samples of different layer thicknesses and materials in one run while other layers remain equal. The layer stack, evaporation rates and treatments of the n-type OPDBTs are: Al 100 nm (2 Å s^{-1})/Cr 10 nm (0.1 Å s^{-1})/i-C_{60} 100 nm (1 Å s^{-1})/Al 15 nm (1 Å s^{-1})/15 min oxidation in ambient air/i-C_{60} 50 nm (1 Å s^{-1})/ Al 15 nm (1 Å s^{-1})/15 min oxidation in ambient air/ i-C_{60} 100 nm (1 Å s^{-1})/ n-C_{60} 20 nm (0.4 Å s^{-1}) co-evaporating C_{60} with W_2 $(hpp)_4$ (purchased from Novaled GmbH, Dresden) using 1 wt.%/two times (perpendicular to each other) SiO 100 nm with a free stripe of 250 µm (1 Å s^{-1})/Cr 10 nm

(0.1 Å s^{-1})/Al 100 nm (2 Å s^{-1}). The layer stack, evaporation rates and treatments of the p-type OPBTs are: Al 100 nm (2 Å s^{-1})/Au 20 nm (0.3 Å s^{-1})/Pentacene:F6TCNNQ 50 nm (0.6 Å s^{-1})/Pentacene 200 nm (2 Å s^{-1})/Al 15 nm (1 Å s^{-1})/15 min oxidation in ambient air/Pentacene 200 nm (2 Å s^{-1})/Pentacene:F6TCNNQ 50 nm (0.6 Å s^{-1})/Au 20 nm (0.3 Å s^{-1})/ Al 100 nm (2 Å s^{-1}). Finally, both n-type and p-type devices are encapsulated under the nitrogen atmosphere (< 1 ppm O_2 and H_2O) using UV cured epoxy glue and cavity glasses without UV exposure of the active area. Annealing of 2 h at 150 °C on a hotplate in a nitrogen glove-box is performed for all n-type OPDBTs. The active areas of the n-type OPDBTs and p-type OPBTs are 250 µm × 250 µm and 2.5 mm × 2.5 mm, respectively.

Device characterization. All electrical measurements are performed at room temperature and in ambient air. Static transfer and output characteristics of the transistors and complementary inverters are carried out using a 5-probe system with a Semiconductor Parameter Analyzer (Keithley 4200-SCS). For all the electrical characterizations, the measurement software SweepMe! (sweep-me.net) is used. A HEWLETT PACKARD 8114A 100V/2A pulse generator, a ROHDE&SCHWARZ HMO3004 4 GSa/s/8 MB Oscilloscope, and a 5-probe system are used to access the dynamic performance of the inverters. High-angle annular dark-field scanning transmission electron microscopy and spectrum imaging analysis based on energy-dispersive X-ray spectroscopy (HAADF-STEM and EDXS) are conducted with a Talos F200X microscope (Thermo Fischer Scientific/FEI, USA) operated at 200 kV and equipped with a Super-X EDX detector, thus providing detailed element maps (O, Al) of the base layer (Supplementary Fig. S1).

Data Availability

The data that support the plots within this paper and other findings of this study are available from the corresponding author upon reasonable request.

Declarations

Acknowledgements

E.G. and S.X. thank the financial support from China Scholarship Council (No.201706890003 and 201706070125). Z.W. acknowledges the Alexander von Humboldt Foundation. K.L. and F.D. gratefully acknowledge the German Research Foundation (DFG) under the grants LE 747/52-2 (SPP FflexCom/Flexartwo). Furthermore, the use of the HZDR Ion Beam Center TEM facilities is gratefully acknowledged.

Author Contributions

Z.W., H.K. and K.L. proposed and supervised the project. E.G., Z.W. and H.K. designed the experiment. E.G., S.X. F.D. and S.W. performed the device characterization. R.H. did the TEM analysis. E.G., Z.W., H.K. and K.L. analyzed the data and co-wrote the manuscript. All authors discussed the results and commented on the manuscript.

Competing Interests

The authors declare no competing interests.

References

1. Chen, Y. *et al.* Flexible active-matrix electronic ink display. *Nature* **423**, 136 (2003).
2. Xu, K., Lu, Y. & Takei, K. Multifunctional skin-inspired flexible sensor systems for wearable electronics. *Adv. Mater. Technol.* **4**, 1800628 (2019).
3. Khan, H. U. *et al.* In situ, label-free DNA detection using organic transistor sensors. *Adv. Mater.* **22**, 4452–4456 (2010).
4. Sekitani, T., Zschieschang, U., Klauk, H. & Someya, T. Flexible organic transistors and circuits with extreme bending stability. *Nat. Mater.* **9**, 1015–1022 (2010).
5. Myny, K. The development of flexible integrated circuits based on thin-film transistors. *Nat. Electron.* **1**, 30–39 (2018).
6. MacPherson, M. R. Threshold shift calaulations for ion implanted MOS devices. *Solid. State. Electron.* **15**, 1319–1326 (1972).
7. Lüssem, B. *et al.* Doped organic transistors operating in the inversion and depletion regime. *Nat. Commun.* **4**, 2775 (2013).
8. Lee, C.-T. & Chen, H.-C. Performance improvement mechanisms of organic thin-film transistors using MoOx-doped pentacene as channel layer. *Org. Electron.* **12**, 1852–1857 (2011).
9. Panidi, J. *et al.* Introducing a nonvolatile n-type dopant drastically improves electron transport in polymer and small-molecule organic transistors. *Adv. Funct. Mater.* **29**, 1902784 (2019).
10. Cui, T. & Liang, G. Dual-gate pentacene organic field-effect transistors based on a nanoassembled SiO 2 nanoparticle thin film as the gate dielectric layer. *Appl. Phys. Lett.* **86**, 064102 (2005).
11. Iba, S. *et al.* Control of threshold voltage of organic field-effect transistors with double-gate structures. *Appl. Phys. Lett.* **87**, 023509 (2005).
12. Gelinck, G. H., Van Veenendaal, E. & Coehoorn, R. Dual-gate organic thin-film transistors. *Appl. Phys. Lett.* **87**, 073508 (2005).
13. Chua, L. L., Friend, R. H. & Ho, P. K. H. Organic double-gate field-effect transistors: Logic-AND operation. *Appl. Phys. Lett.* **87**, 253512 (2005).
14. Morana, M., Bret, G. & Brabec, C. Double-gate organic field-effect transistor. *Appl. Phys. Lett.* **87**, 153511 (2005).
15. Spijkman, M. *et al.* Increasing the noise margin in organic circuits using dual gate field-effect transistors. *Appl. Phys. Lett.* **92**, 143304 (2008).
16. Myny, K. *et al.* Unipolar organic transistor circuits made robust by dual-gate technology. *IEEE J. Solid-State Circuits* **46**, 1223–1230 (2011).
17. Klauk, H. Will we see gigahertz organic transistors? *Adv. Electron. Mater.* **4**, 1700474 (2018).

18. Greenman, M., Yoffis, S. & Tessler, N. Complementary inverter from patterned source electrode vertical organic field effect transistors. *Appl. Phys. Lett.* **108**, 1–5 (2016).
19. Kleemann, H., Krechan, K., Fischer, A. & Leo, K. Review of vertical organic transistors. *Adv. Funct. Mater.* **30**, 1907113 (2020).
20. Dollinger, F. *et al.* Vertical organic thin-film transistors with an anodized permeable base for very low leakage current. *Adv. Mater.* **31**, 1900917 (2019).
21. Lim, K. G. *et al.* Anodization for simplified processing and efficient charge transport in vertical organic field-effect transistors. *Adv. Funct. Mater.* **30**, 2001703 (2020).
22. Guo, E. *et al.* High-performance static induction transistors based on small-molecule organic semiconductors. *Adv. Mater. Technol.* 2000361 (2020) doi:10.1002/admt.202000361.
23. Lenz, J., del Giudice, F., Geisenhof, F. R., Winterer, F. & Weitz, R. T. Vertical, electrolyte-gated organic transistors show continuous operation in the MA cm−2 regime and artificial synaptic behaviour. *Nat. Nanotechnol.* **14**, 579–585 (2019).
24. Perinot, A. & Caironi, M. Accessing MHz operation at 2 V with field-effect transistors based on printed polymers on plastic. *Adv. Sci.* **6**, 1801566 (2019).
25. Ben-Sasson, A. J. *et al.* Patterned electrode vertical field effect transistor fabricated using block copolymer nanotemplates. *Appl. Phys. Lett.* **95**, 213301 (2009).
26. Ben-Sasson, A. J. *et al.* Self-assembled metallic nanowire-based vertical organic field-effect transistor. *ACS Appl. Mater. Interfaces* **7**, 2149–2152 (2015).
27. Subedi, K. N., Al-Shadeedi, A. & Lüssem, B. Stability of organic permeable base transistors. *Appl. Phys. Lett.* **115**, 193301 (2019).
28. Kaschura, F., Fischer, A., Kasemann, D., Leo, K. & Lüssem, B. Controlling morphology: A vertical organic transistor with a self-structured permeable base using the bottom electrode as seed layer. *Appl. Phys. Lett.* **107**, 033301 (2015).
29. Kheradmand-Boroujeni, B. *et al.* A pulse-biasing small-signal measurement technique enabling 40 MHz operation of vertical organic transistors. *Sci. Rep.* **8**, 7643 (2018).
30. Dollinger, F. *et al.* Electrically stable organic permeable base transistors for display applications. *Adv. Electron. Mater.* **5**, 1900576 (2019).
31. Lüssem, B. *et al.* Doped organic transistors. *Chem. Rev.* **116**, 13714–13751 (2016).
32. Guo, E. *et al.* Vertical organic permeable dual-base transistors for logic circuits. *Nat. Commun.* Forthcoming (2020) doi:10.1038/s41467-020-18576-5.
33. Klinger, M. P. *et al.* Organic power electronics: transistor operation in the kA/cm2 regime. *Sci. Rep.* **7**, 44713 (2017).
34. Dao, T. T. *et al.* Controllable threshold voltage in organic complementary logic circuits with an electron-trapping polymer and photoactive gate dielectric layer. *ACS Appl. Mater. Interfaces* **8**, 18249–18255 (2016).

35. Yoo, H., On, S., Lee, S. B., Cho, K. & Kim, J. J. Negative transconductance heterojunction organic transistors and their application to full-swing ternary circuits. *Adv. Mater.* **31**, 1808265 (2019).
36. Shiwaku, R. *et al.* Printed organic inverter circuits with ultralow operating voltages. *Adv. Electron. Mater.* **3**, 1600557 (2017).
37. Borchert, J. W. *et al.* Flexible low-voltage high-frequency organic thin-film transistors. *Sci. Adv.* **6**, eaaz5156 (2020).

Figures

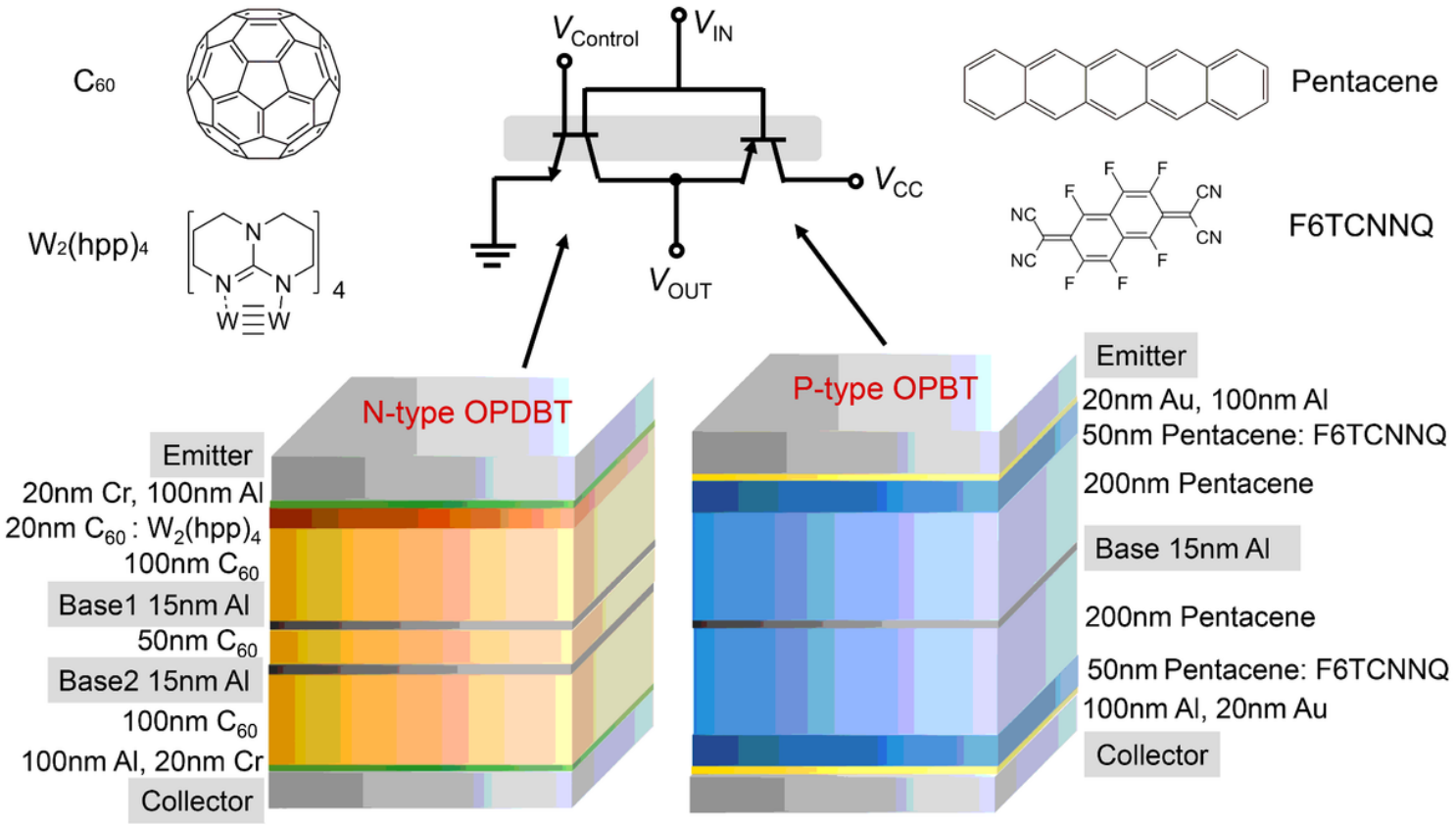

Figure 1

Circuit design. Circuit diagram, chemical molecular structures, and schematic cross-section of the organic complementary inverters.

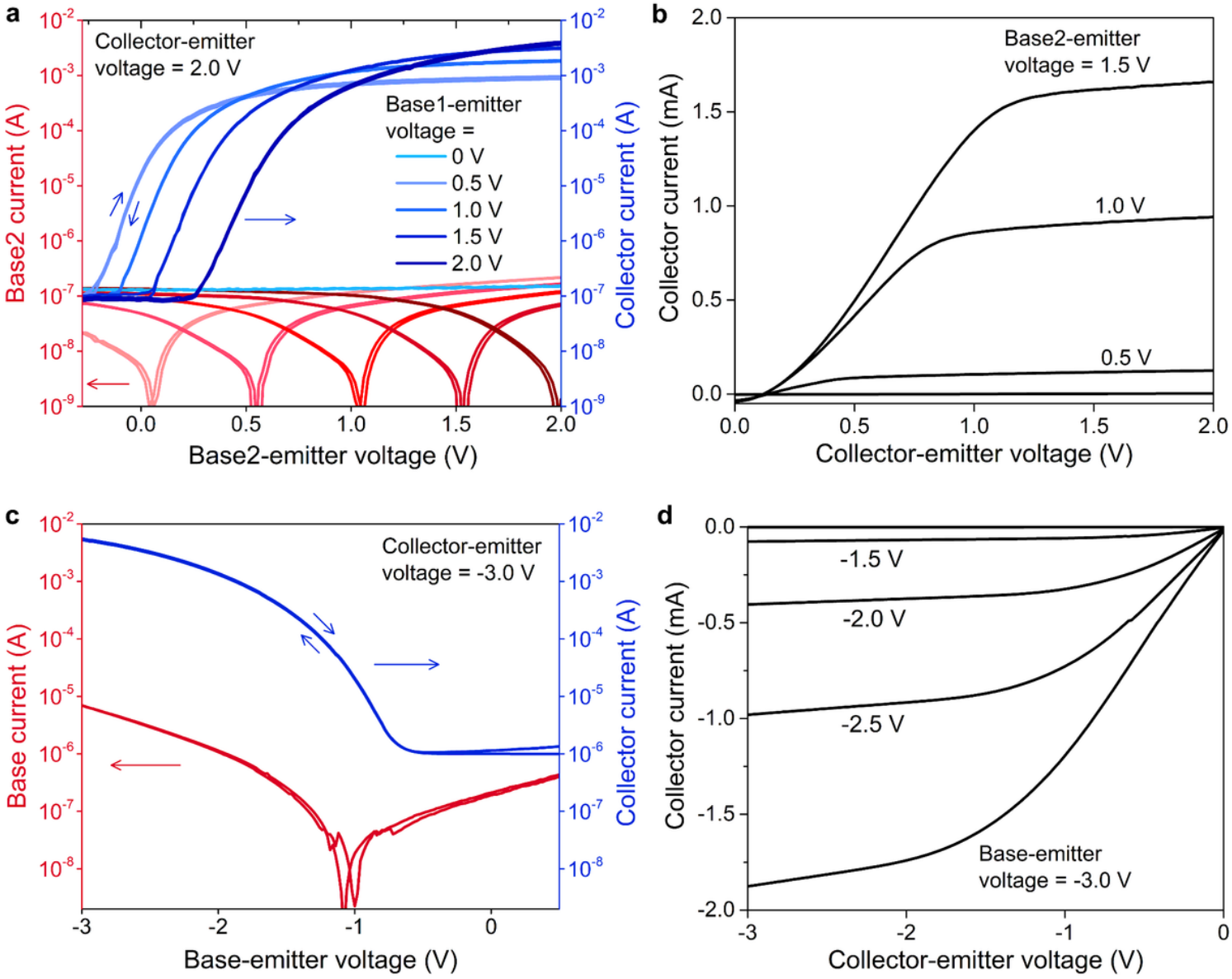

Figure 2

Static transistor characteristics. a) Transfer characteristics of an n-type OPDBT as a function of base2-emitter voltage VB2 at different base1-emitter voltages VB1 of 0, 0.5, 1.0, 1.5 and 2.0 V, respectively. b) Output characteristics of the same n-type OPDBT measured at a VB1 of 2.0 V and VB2 of 0, 0.5, 1.0, 1.5 and 2.0 V, respectively. c) Measured transfer curves of a p-type OPBT as a function of base-emitter voltage with a collector-emitter voltage VCE of -3.0 V. d) Measured output characteristics of the same p-type OPBT.

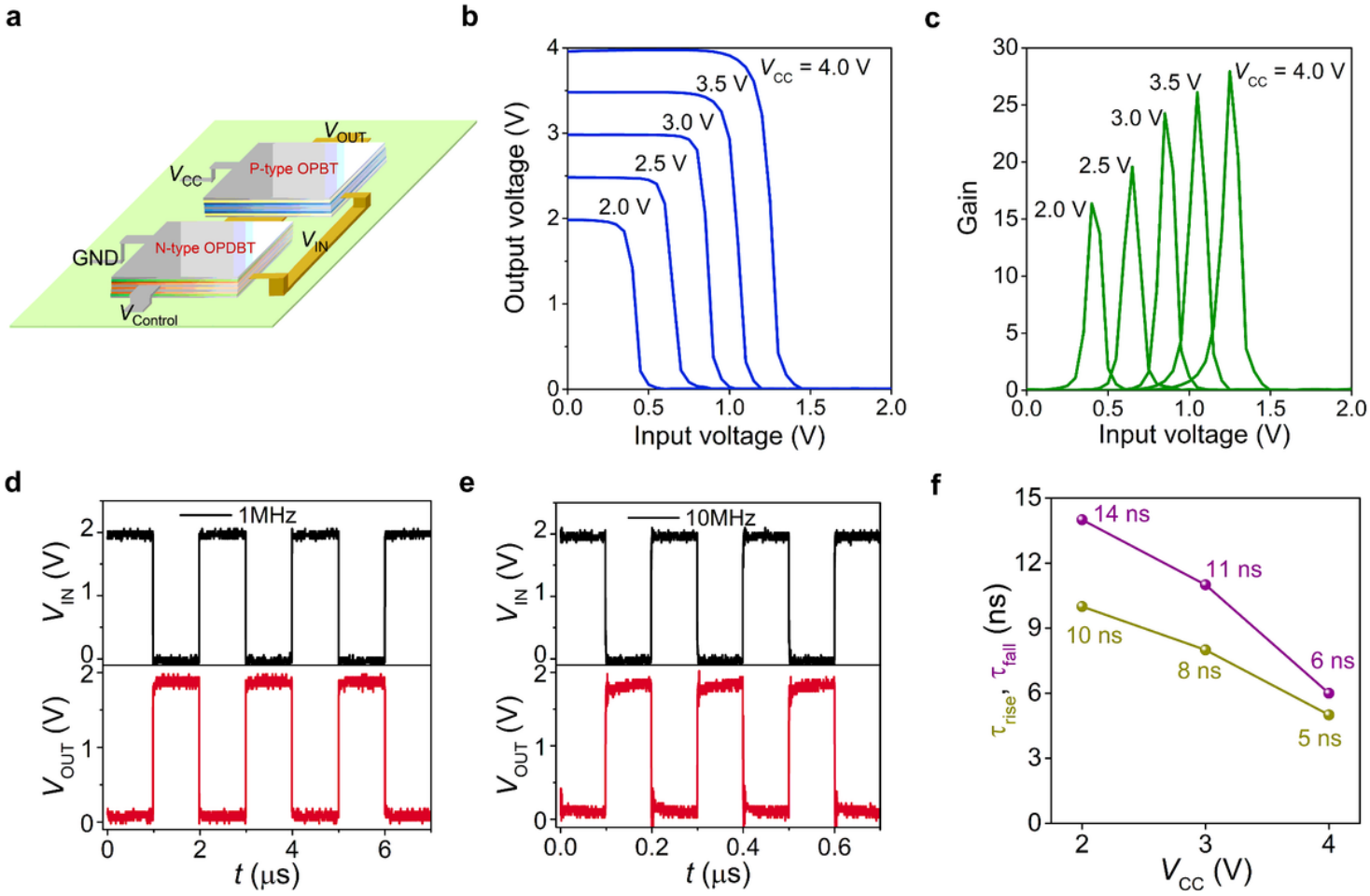

Figure 3

Static and dynamic inverter characteristics. a) Schematic diagram and photograph of an organic complementary inverter. b) Static transfer characteristics, and c) the corresponding gain of the organic complementary inverter measured at a VControl of 2.0 V and the VCC of 2.0, 2.5, 3.0, 3.5 and 4.0 V, respectively. d,e) Dynamic characteristics of the same inverter in response to a square-wave input signal with an amplitude of 2.0 V and a frequency of (d) 1 MHz and (e) 10 MHz. f) Rise and fall time constants of the switching delays measured for VCC of 2.0, 3.0 and 4.0 V.

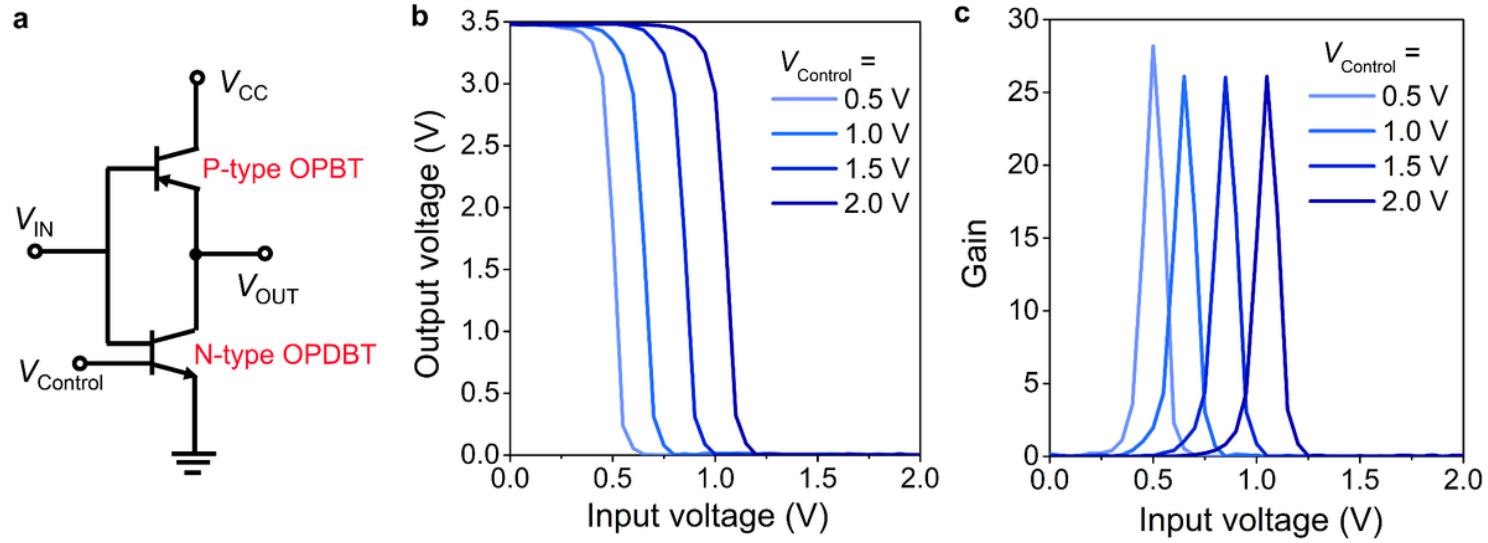

Figure 4

Switching voltage control. a) Circuit diagram, b) static transfer characteristics, and c) the corresponding gain of the organic complementary inverter measured for VCC of 3.5 V and VControl of 0.5, 1.0, 1.5 and 2.0 V, respectively.